Nanomechanics of Flexoelectric Switching

J. Očenášek,[1*] H. Lu,[2*] C. W. Bark,[3] C. B. Eom,[3] J. Alcalá,[4] G. Catalan,[5,6] and A. Gruverman[2]

[1]*New Technologies Research Centre, University of West Bohemia in Pilsen, 30614 Plzeň, Czech Republic.*

[2]*Department of Physics and Astronomy, University of Nebraska-Lincoln, NE 68588, USA*

[3]*Department of Materials Science and Engineering, University of Wisconsin-Madison, WI 53706, USA*

[4]*Department of Materials Science and Metallurgical Engineering, GRICCA, EUETIB and ETSEIB Universitat Politecnica de Catalunya, Barcelona, Spain*

[5]*Institut Catala de Recerca i Estudis Avançats (ICREA), Catalunya, Spain*

[6]*Institut Catala de Nanociencia i Nanotecnologia (ICN2), Campus UAB, Bellaterra, Barcelona, Spain*

[*] These authors contributed equally to this work

ABSTRACT

We examine the phenomenon of flexoelectric switching of polarization in ultrathin films of barium titanate induced by a tip of an atomic force microscope (AFM). The spatial distribution of the tip-induced flexoelectricity is computationally modelled both for perpendicular mechanical load (point measurements) and for sliding load (scanning measurements), and compared with experiments. We find that (i) perpendicular load does not lead to stable ferroelectric switching in contrast to the load applied in the sliding contact load regime, due to non-trivial differences between the strain distributions in both regimes: ferroelectric switching for the perpendicular load mode is impaired by a strain gradient inversion layer immediately underneath the AFM tip; while for the sliding load regime, domain inversion is unimpaired within a greater material volume subjected to larger values of the mechanically induced electric field that includes the region behind the sliding tip; (ii) beyond a relatively small value of an applied force, increasing mechanical pressure does *not* increase the flexoelectric field inside the film, but results instead in a growing volume of the region subjected to such field that aids domain nucleation processes; and (iii) the flexoelectric coefficients of the films are of the order of few nC/m, which is much smaller than for bulk $BaTiO_3$ ceramics, indicating that there is a "flexoelectric size effect" that mirrors the ferroelectric one.

Submitted to Physical Review B, April 2015.

I. INTRODUCTION

Ferroelectric materials are characterized by the presence of a spontaneous polarization that can be switched by application of an external electric field. Recently, a mechanical switching of polarization was also demonstrated.[1] The driving mechanism of the mechanically-induced polarization switching is thought to be the flexoelectric effect [2] – a linear coupling between polarization and a strain gradient, which allows control of not only the polarization magnitude but also its orientation. In bulk materials, flexoelectric effects are generally small because large strain gradients are difficult to achieve without fracture or permanent deformation. Conversely, at the nanoscale, strain gradients can acquire extremely large magnitudes leading to giant flexoelectric effects. [3-5] The importance of flexoelectricity for nanodevices has largely contributed to the current surge of interest in this effect that had been known for nearly half a century.[2,6]

Despite considerable research in the last decade (see several monographic reviews for reference [7-10]) the true magnitude and nature of the flexoelectric coefficients of most materials is only now beginning to be understood.[11-14] Crucially, it is not known whether the large flexoelectric coefficients of archetypal ceramics such as $BaTiO_3$ (BTO) remain equally large at the nanoscale. This is a critical question because it is at the nanoscale where gradient-induced effects are most important and likely to be useful, so, if we are to exploit them, we need to know the flexoelectric coefficients at the nanoscale. These may not necessarily be the same as in bulk: note, for example, that the dielectric constant of ferroelectric thin films is much smaller than that of bulk, and flexoelectricity is linearly proportional to permittivity.[2] Our work seeks to answer this question, namely: can we quantify the value of the flexoelectric coefficients in ferroelectric thin films? We demonstrate that reasonable fitting of the experimental results in $BaTiO_3$ thin films can be achieved only for flexoelectric coefficients of the order of 1 nC/m. This is in contrast to bulk $BaTiO_3$, where the flexoelectric coefficients are of the order of 1 μC/m, confirming that there is indeed a "flexoelectric size effect" that mirrors the ferroelectric one.

Of equal importance for understanding the mechanically-induced ferroelectric switching is the analysis of the actual distribution of the strain gradient. Strain and stress fields produced by a tip of an atomic force microscope (AFM) are much more complex than those associated with pure bending or twisting, and can lead to non-trivial physical effects. In this work, we have established that (i) the mechanical switching process is controlled by critical domain size rather than by critical field; and that

(ii) there is a fundamental difference in the strain gradient distributions generated in the normal and sliding load modes so that the former leads to small and unstable domains while the latter results in more stable domains.

II. EXPERIMENTS

We have quantified the flexoelectric behavior in ultrathin BTO films by establishing a correlation between the mechanical load and equivalent electric bias. The samples studied were single-crystalline epitaxial ultrathin BTO films, grown on atomically smooth TiO_2-terminated (001)-$SrTiO_3$ substrate with a 30-nm-thick $La_{0.67}Sr_{0.33}MnO_3$ layer acting as bottom electrode. Both layers were grown using pulsed laser deposition with *in situ* monitoring using high pressure reflection high energy electron diffraction (RHEED) for thickness control; details of sample preparation can be found elsewhere.[1] The switching experiments were performed on 12-unit-cell(u.c.)-thick films (~5 nm). The compressively-strained BTO thin films were fully coherent with the substrate and possessed only out-of-plain polarization.[15] The flexoelectric switching was studied using a commercial AFM system (MFP-3D, Asylum Research).

Flexoelectric measurements have been performed using two modes of mechanical pressure induced by the AFM tip. In one mode – the sliding contact load mode – the BTO film surface has been scanned with the tip under an incrementally increasing loading force from 100 nN to 1000 nN, while applying a DC voltage to the tip (this bias ranging from -0.4V to 1.2V was fixed during scanning). Note that for all measurements the external DC bias was below the coercive bias estimated from the PFM hysteresis loop (1.2 V for 12-u.c.-thick film[1]) and by itself could not cause polarization reversal. Scanning under mechanical load was followed by visualization of the resulting domain patterns using conventional piezoresponse force microscopy (PFM) with a low load force of 25 nN. In the normal load mode, we have used an AFM tip at a fixed position on the BTO film surface to measure the local PFM hysteresis loops for different values of the loading forces.

In Fig. 1(a), it can be seen that application of an increasing force in the sliding contact load mode eventually leads to the reversal of the initial upward (away from the electrode) polarization state to the downward state. The threshold force, at which the PFM phase contrast in Fig. 1(a) is inverted (which

also corresponds to the minimum in the PFM amplitude), varies with the applied DC bias, i.e. the force required for switching the polarization from "up" to "down" decreases or increases, respectively, depending on whether the voltage applied to the tip is positive or negative.

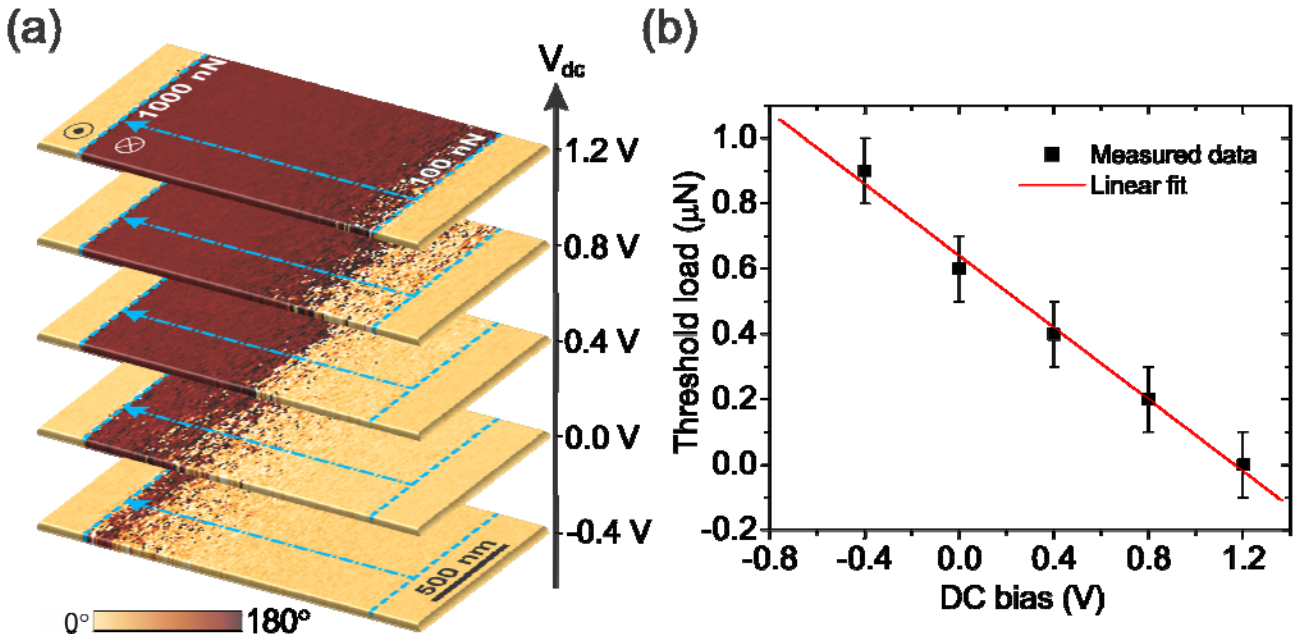

FIG. 1. (a) PFM phase images of 12-u.c.-thick $BaTiO_3$ film after mechanical writing in the area marked by the lines with at a fixed DC voltage V_{ex} applied to the tip. Mechanical load was increasing during scanning from 100 nN to 1000 nN in the direction marked by a dashed arrow. Polarization switches downward as mechanical load increases. Positive DC bias assists polarization switching to the downward direction and negative DC bias opposes it. The threshold load is defined as a load at which phase contrast is inverted. (b) A plot of the threshold load F_{th} as a function of the tip voltage obtained using data in (a).

We interpret these results in terms of cooperation or competition between the external electric bias and the mechanically-induced voltage. This mechanical voltage is an effective measure of the complex electric field produced by pressure-induced piezoelectricity plus the strain-*gradient*-induced flexoelectricity, which varies depending on film thickness, loading mode (sliding vs. perpendicular contacts) and tip conductivity. Notice, however, that the piezoelectric contribution always reduces the coercive voltage due to the vertical pressure-induced reduction of tetragonality,[16] whereas the flexoelectric contribution can either increase or decrease the required external coercive voltage depending on whether the flexoelectric polarization is parallel or antiparallel to the ferroelectric polarity.

Note also that, since the piezoelectric effect can only reduce preexisting polarity, it cannot cause ferroelectric switching, meaning that mechanical switching of polarization is controlled by the flexoelectric contribution. The condition for mechanically-induced switching can be expressed as $V_{fl}(F) \geq V_c$, where $V_{fl}(F)$ is the flexoelectric voltage for a given value of the tip-applied mechanical force F and V_c is the coercive voltage of the film. At the threshold load F_{th} the flexoelectric voltage is equal to the coercive bias: $V_{fl}(F_{th}) = V_c$. When a small (below V_c) external DC voltage V_{ex} is applied during mechanical writing, the general condition for polarization reversal can be expressed as $V_{fl}(F) + V_{ex} \geq V_c$ so that the flexoelectric voltage corresponding to the threshold load can be found from $V_{fl}(F_{th}) + V_{ex} = V_c$. By measuring the threshold load F_{th} as a function of the external voltage V_{ex}, we establish a relationship between the applied load F and the flexoelectrically-generated voltage V_{fl}. A plot in Fig. 1(b) shows a linear relationship between the external DC bias V_{ex} and the threshold load F_{th} with a proportionality coefficient of 1.8 V/μN.

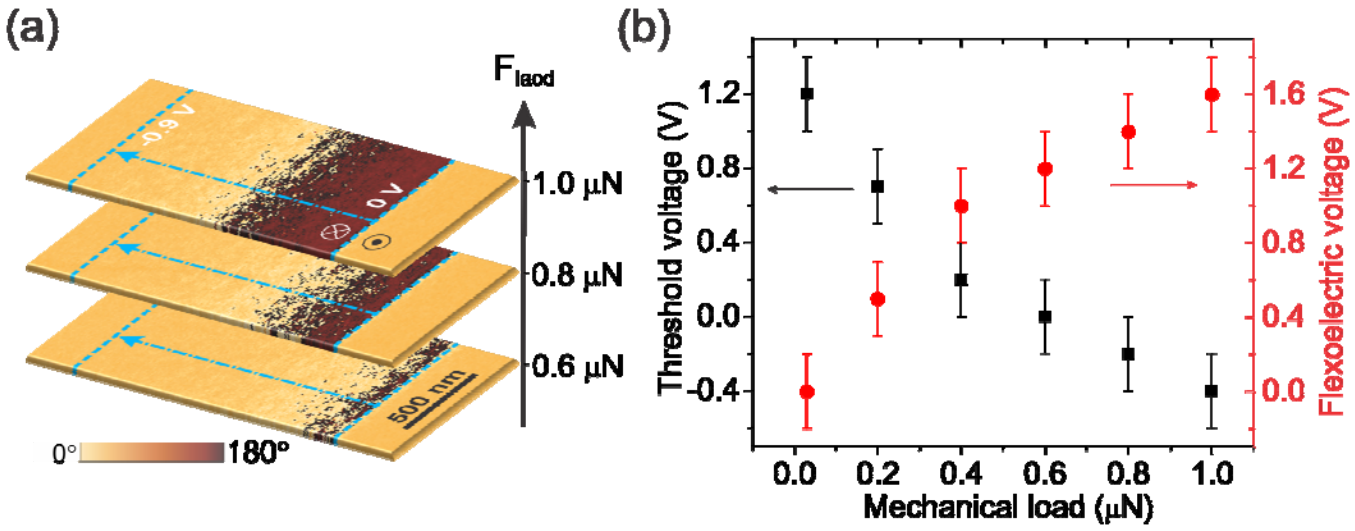

FIG. 2. (a) PFM phase images of 12-u.c.-thick $BaTiO_3$ film after electrical writing at a fixed mechanical load in the area marked by the dashed lines. Electrical bias was changing during scanning in the direction marked by a dashed arrow. Polarization switching is stopped as negative DC bias increases. (b) Plots of the experimentally measured threshold voltage bias and calculated flexoelectric voltage as a function of the mechanical load. For mechanical load below 600 nN, an increasing positive bias is applied to induce polarization switching.

An alternative and somewhat more direct way to calibrate the flexoelectric voltage is based on scanning the film surface with incrementally increasing a DC bias applied to the tip while maintaining a constant mechanical load. In this case switching to the upward polarization state will occur at the threshold DC bias V_{th}, which is measured experimentally, and the flexoelectric voltage can be found from $V_{fl}(F) + V_{th} = V_c$. At the mechanical load close to zero, $V_{fl} = V_c$ (in reality, we take the value of V_{th} at the mechanical load of 30 nN as being equal to V_c). A series of the domain patterns generated using this approach are shown in Fig. 2(a) while Fig. 2(b) shows the threshold voltage V_{th} and the calculated flexoelectric voltage V_{fl} as a function of mechanical load F. It can be seen that V_{th} decreases monotonically as mechanical load increases, and even becomes negative at a sufficiently high load, indicating that the tip-generated flexoelectric voltage becomes larger than V_c. A slight nonlinearity of the slope is this case is likely caused by tip wear. Note that at the load of 600 nN, the external voltage required to switch the polarization is exactly $V_{ex} = 0$: this implies that, at this mechanical load, the flexoelectric voltage equals the coercive voltage of the film.

The above measurements have been performed in the scanning mode, where in addition to the normal force, friction between the tip and the film generates tangential forces. It is useful to compare these results with those of measurements done in the other mode - normal loading mode, where the load is applied through a tip fixed at a certain point on the surface. In this case, the tangential forces are absent. Experimentally, however, we found that perpendicular indentation leads to small and unstable domains, so graphic analysis of polarization maps such as those of Fig. 1 was not possible. Instead, we have analysed the point-measurements of the PFM hysteresis loops obtained at different loading forces. In Fig. 3(a), it can be seen that with increase in the loading force the PFM loops become more asymmetric and shift along the horizontal axis (bias) toward the negative voltages. Both the shift and the asymmetry are necessarily associated with the strain gradients. The off-centering of the loop, just like in the scanning mode, is a direct measure of the flexoelectrically-induced voltage, while the asymmetry of the PFM loop wings reflects the fact that the PFM signal is amplified when ferroelectric and strain-induced (flexoelectric) polarizations are parallel (i.e. when the total polarization of the film is high) and reduced when they are antiparallel.

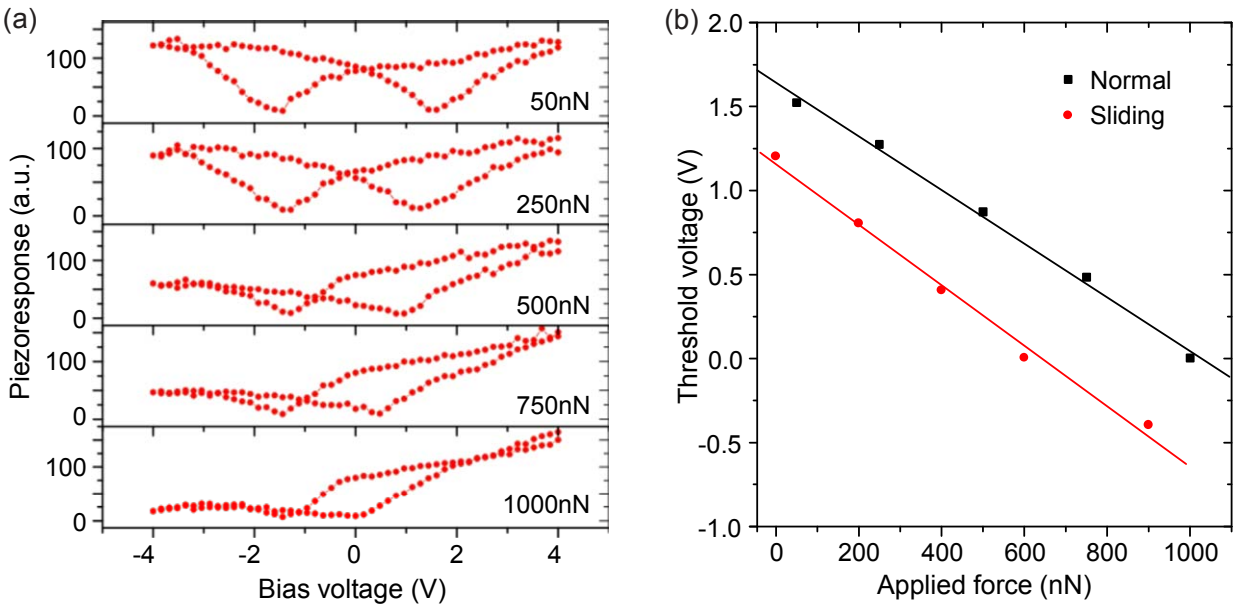

FIG. 3. (a) PFM hysteresis loops acquired under different normal loading forces. Note that for the highest force, one of the coercive voltages is zero, indicating that the mechanically-induced bias is sufficient to switch to the downward state. (b) Comparison between the threshold voltages required for switching polarization from the upward to the downward state for sliding (scanning) and normal load modes.

In Fig. 3(b) we plot the applied force dependence of the threshold voltage for two different loading regimes. In the normal load regime, the threshold voltage is always higher, indicating that sliding contacts are more efficient in generating flexoelectric voltage and inducing ferroelectric switching. The conversion factor from force into voltage is about 1.8 V/μN for both regimes. The reasons for this difference will be discussed in the next section.

III. SIMULATIONS

In order to explain the experimental observations, it is necessary to calculate the tip-induced strain gradients, associated flexoelectric polarizations and electrostatic field distributions. For this, we turn to finite element (FE) simulations performed for a spherical elastic contact between a rigid AFM tip with radius of 30 nm (consistent with the value measured with high-resolution field-emission SEM for

the tips used in the experiments) and a 12-u.c.-thick BTO film on a $La_{0.67}Sr_{0.33}MnO_3$ substrate. We used elastic stiffness moduli C_{11} = 166 GPa, C_{12} = 76 GPa and C_{44} = 42 GPa for BTO [17] and C_{11}=180 GPa, C_{12} = 100 GPa and C_{44} = 56 GPa for $La_{0.67}Sr_{0.33}MnO_3$.[18] For simplicity, the $La_{0.67}Sr_{0.33}MnO_3$ interlayer used as electrode is assumed to be infinitely thick, which approximates sufficiently well to the elastic boundary condition of the experiments. Complementary simulations were performed for the case of the 12-u.c.-thick BTO film placed on top of a much stiffer $SrTiO_3$ (STO) substrate with C_{11} = 421 GPa, C_{12} =122.1 GPa, C_{44} =133.2 GPa. The purpose of these simulations was to assess the role of an increased elastic contrast between the film and the substrate in flexoelectric nanocontacts. Normal as well as sliding loading modes were modelled under increasing applied loads up to a maximum of 1000 nN. Coulombian friction coefficients μ = 0, 0.2 and 0.3 were considered in the modelling of sliding contacts.[19-21]

The following scheme was employed. The strain gradients were first computed from the nodal values in the FE mesh while the strain gradients were computed by recourse to the shape functions of the quadrilateral elements. Linear flexoelectricity was then invoked, providing all strain gradients in the film, such that

$$P_i = \mu_{ijkl}\, e_{jk,l} \qquad \text{Eq. (1)}$$

where P_i is the polarization vector along the i-axis, $e_{jk,l}$ is the derivative along the x_l direction of the lagrangian strain tensor, μ_{ijkl} is the fourth-rank tensor of flexoelectric coefficients and subindices i,j,k,l vary from 1 to 3. In all tensor coefficients in this article, x_1 and x_2 are the in-plane directions, and x_3 is the out of plane (indentation) direction. Following the analysis outlined in the Appendix, the components of the polarization vector along the three material axes become

$$P_1 = \mu_{1111}\frac{\partial e_{11}}{\partial x_1} + \mu_{1122}\left(\frac{\partial e_{22}}{\partial x_1} + \frac{\partial e_{33}}{\partial x_1}\right) + 2\mu_{1212}\left(\frac{\partial e_{12}}{\partial x_2} + \frac{\partial e_{13}}{\partial x_3}\right) \qquad \text{Eq. (2a)}$$

$$P_2 = \mu_{1111}\frac{\partial e_{22}}{\partial x_2} + \mu_{1122}\left(\frac{\partial e_{11}}{\partial x_2} + \frac{\partial e_{33}}{\partial x_2}\right) + 2\mu_{1212}\left(\frac{\partial e_{12}}{\partial x_1} + \frac{\partial e_{23}}{\partial x_3}\right) \qquad \text{Eq. (2b)}$$

$$P_3 = \mu_{1111}\frac{\partial e_{33}}{\partial x_3} + \mu_{1122}\left(\frac{\partial e_{11}}{\partial x_3} + \frac{\partial e_{22}}{\partial x_3}\right) + 2\mu_{1212}\left(\frac{\partial e_{13}}{\partial x_1} + \frac{\partial e_{23}}{\partial x_2}\right) \qquad \text{Eq. (2c)}$$

The flexoelectric coefficients μ_{ijkl} are not known with certainty, and even for bulk single crystals there are orders of magnitude discrepancies between experiment and theory. Here, we use the more conservative theoretical results from the first-principles calculations: μ_{1111} = 0.37 nC/m,[22] μ_{1122} = 5.5 nC/m,[23] and μ_{1212} = 1.9 nC/m;[23] this choice is validated by comparison with our experimental results. The small value of the flexoelectric coefficients for thin films is precisely one of the central results of this work.

Since the entire strain gradient field is known from the above simulations, the charge density at all nodal points of the FE mesh representing the BTO film are subsequently computed through

$$q = -\nabla \cdot P_i \quad . \qquad \text{Eq. (3)}$$

Such charge density distribution is then introduced in a final finite element analysis where Maxwell's equations are solved for the electrical boundary conditions imposed by the spherical tip, thus providing the total three-dimensional electric field inside the thin film. In doing so, we assume that the relative permittivity of the film, ε_r = 30 (see Section IV.C). In the latter computations, the substrate is grounded and the indenter is taken to exhibit either conductive or insulating properties. In the case of conductive tips, Maxwell's equations are solved for imposed boundary voltage values ranging from -1.0 to +1.0 V (in steps of 0.1V). Boundary voltage conditions at the contact surface are not imposed when modelling the response of insulating tips.

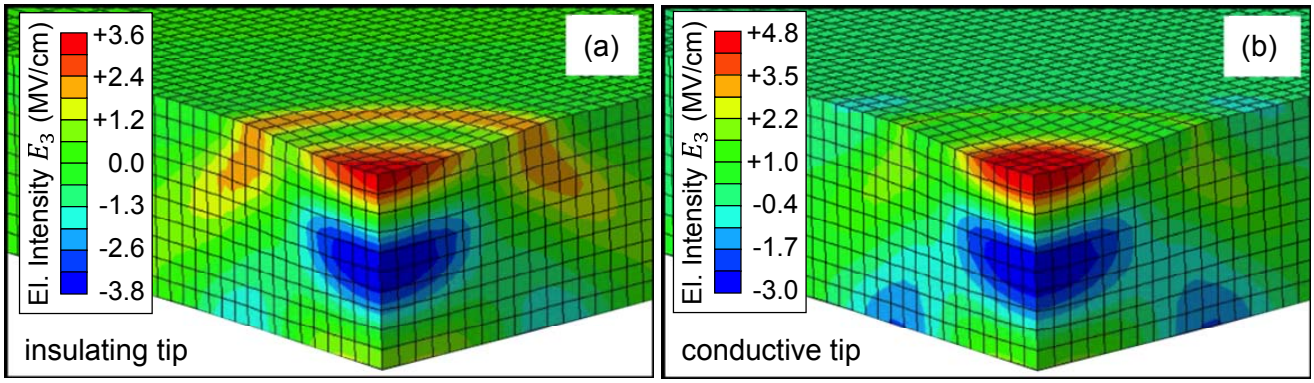

FIG. 4. Isocontours of the total field in the vertical direction (E_3) for an applied contact load of 500 nN (normal mode). (a) Insulating (non-screening) tip and (b) conductive tip at 0 V of imposed bias. Regions colored in red indicate presence of strain gradients opposing domain switching whereas the maximum flexoelectric field value

E_p is located at the central region colored in blue. The size of one quadrilateral element matches that of 1 u.c. in $BaTiO_3$. The same color code is used in (a) and (b).

Figure 4 shows the flexoelectric field distribution under the tip, for insulating and conductive tips. In both cases, the peak value of the negative (downward oriented) electric field, E_p, in the vertical x_3 direction is found at $0.6r$ underneath the center of contact, where r is the contact radius. Immediately underneath the tip apex, however, a strong positive (upward) field is induced, which opposes domain inversion (note the region colored in red in Fig. 4). This region of inversion probably explains the observed instability of domains written by pure normal indentation. The maximum downward field value, E_p, is 20% smaller for conductive than that for insulating tips under the same applied indentation load, demonstrating the sensitivity of the flexoelectric field to the electrical boundary condition, and suggesting that insulating tips may in fact be better for purely mechanical switching.

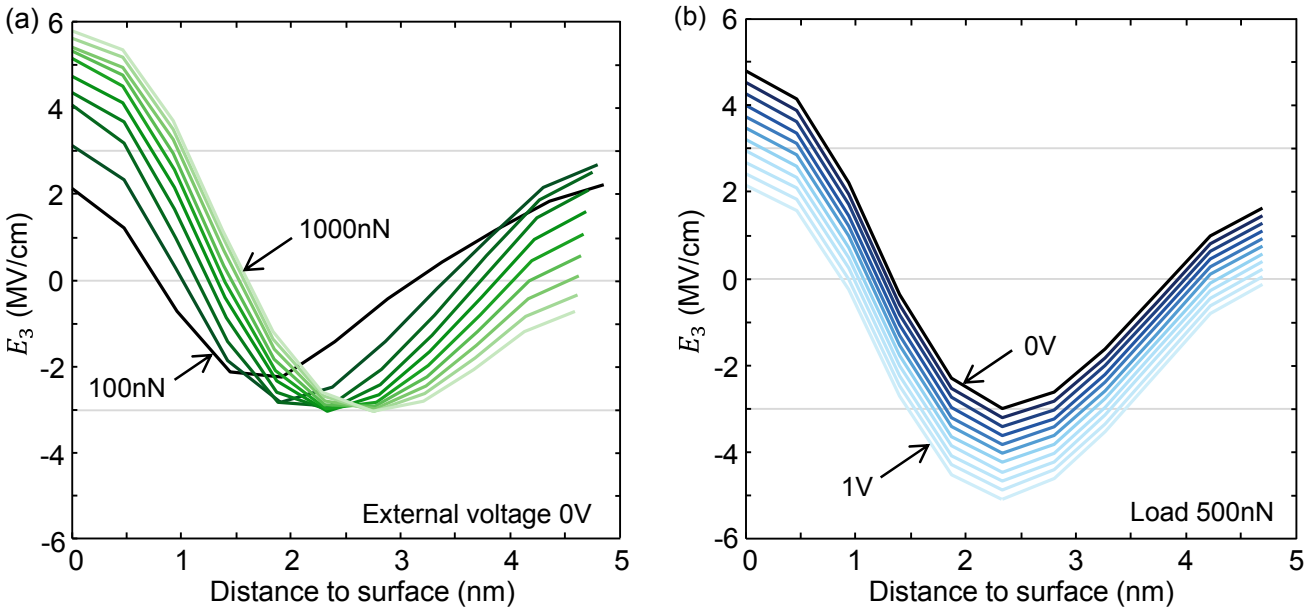

FIG. 5. Distributions of the electric field E_3 along a vertical path underneath the contact center for the normal load regime using a conductive tip. Part (a) shows that, in the absence of external voltage, the peak negative field E_p is almost the same (~3 MV/cm) for any value of mechanical load. (b) Influence of the external voltage upon the distributions of total field for the mechanical load of 500 nN. Consecutive curves are 100 nN apart in (a) and 0.1 V apart in (b).

The field distribution along the vertical direction directly under the tip apex, plotted in Fig. 5, also shows that, for any given normal mechanical load, the contact area is under a positive (upward oriented) field while a negative field is concentrated a couple of nanometers below. A key finding (Fig. 5(a)) is that increasing mechanical load does not result in a stronger negative field, but in a larger volume fraction of the film being subjected to such negative field, thus indicating that the switching is controlled by critical nucleus size rather than by intensity of local field. By contrast, if we increase the external voltage while maintaining a fixed amount of pressure (Fig. 5(b)), both the nucleus size and the intensity of the negative field do increase. Mechanical load and applied voltage thus generate very different field distributions.

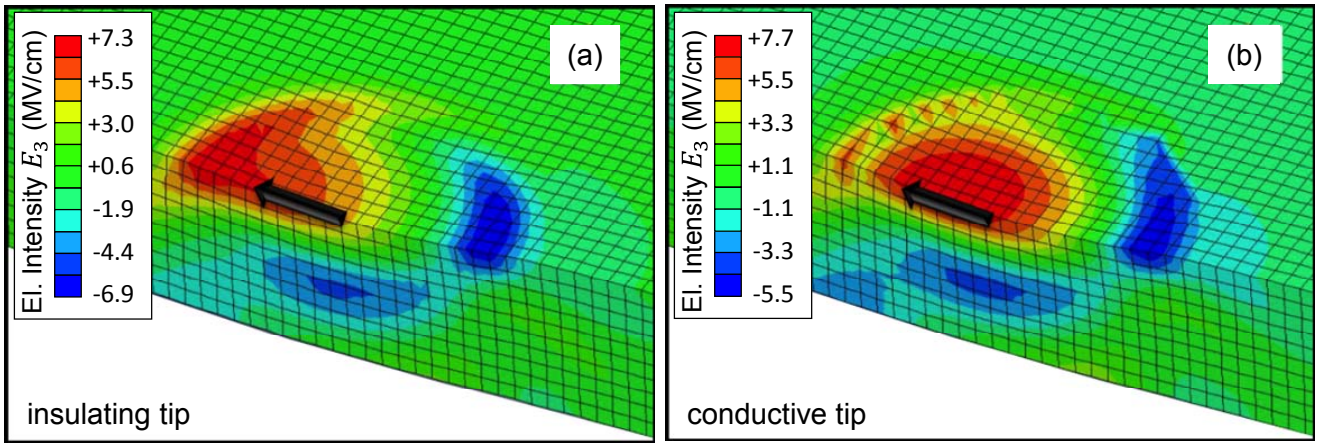

FIG. 6. Isocontours of total electric field E_3 for a sliding contact load regime for (a) isolating tip and (b) conductive tip at 0 V of applied voltage. Simulations are made for the Coulombian friction coefficient μ = 0.3 and vertical load of 500 nN. Black arrow denotes the sliding direction. The strain gradients in the regions colored in red produce positive (upward) electric field, which opposes flexoelectric switching, while domain nucleation occurs under the negative field (blue regions). The size of one quadrilateral element matches that of 1 u.c. in $BaTiO_3$. The same color code is used in (a) and (b).

Meanwhile, the field distribution for the sliding contact load regime (Fig. 6) shows a qualitatively new and very important feature: the negative flexoelectric field exists both underneath the tip-sample contact point (as described above) *and* in the material volume trailing behind the sliding tip (Fig. 6). Importantly, while the region of negative field vertically under the tip is still partially offset by

the positive field in the contact region, the trailing negative field induced under sliding conditions is not offset by any positive field and should thus prevail. Moreover, for sliding contacts with Coulomb's friction coefficient of $\mu = 0.3$, the E_p value underneath the tip increased by ~ 50% as compared to that developing for perpendicular contacts, and in addition the material volume subjected to the peak E_p level is three times greater for the sliding mode. These results thus explain the greater ease with which stable domains can be written in sliding mode compared to perpendicular indentation.

IV. DISCUSSION

The principal features of the experiment (magnitude of the effect, greater writing ability for sliding as compared to normal indentation) are well reproduced and explained by the computations. There are, however, a few aspects that require further discussion, namely: (i) flexoelectric switching appears to occur due to the expansion of the downwardly polarized region beyond a certain critical volume rather than due to the increase in the strength of the downward oriented flexoelectric field; (ii) the maximum applied loads are high enough to induce a localized transition to the paraelectric phase; and (iii) though the order of magnitude of the flexoelectric coefficients is known, the accuracy and relative weight of the different flexoelectric components needs to be examined. We discuss these issues in this section.

A. Domain nucleation and critical volume for polarization reversal

Switching in ferroelectrics proceeds through domain nucleation and growth:[24-27] nucleation of a critical domain size with downward polarization precedes overall switching across the film thickness so that the free energy of the film is reduced as the nucleated domain expands. Our simulations show that an increase in applied mechanical load results in a greater material volume subjected to the peak value of the flexolectric field E_p. Experimentally, we know that the coercive voltage in the (relative) absence of pressure is approximately 1.5 V (corresponding to 3 MV/cm of electrical field). In our simulations (Fig. 4), this field value defines an isocontour of $0.9 \times E_p$, circumscribing a material volume of ~ 4 nm^3. For spherical nuclei, this volume translates to a critical radius $r_c \sim 1.0$ nm that encompasses ~ 32 unit cells.

Following the analysis in Ref 26, the thermodynamics of domain nucleation processes is described by

$$U = -2PEv + \gamma_s s + U_d \qquad \text{Eq. (4)}$$

where U is the total free energy of the film; the first term in the right-hand side is the energy decrease driving domain nucleation, which contains the magnitudes of the electric field E and polarization P within a nucleated domain with volume v; γ_s is the surface energy of the domain walls for nuclei with surface area s; and U_d is the depolarization energy imposed by the surrounding material. The saddle point in the energy landscape therefore describes the critical radius of the nucleated domain in accordance with $(dU/dr) = 0$. For nuclei with spherical shape, the critical domain radius becomes

$$r_c = \gamma_s/PE \qquad \text{Eq. (5)}$$

Using the computed peak values of E_p, associated P and γ_s=17 mJ/m^2 for domain walls in $BaTiO_3$,[26,28] Eq. (5) yields $r_c \sim$ 0.4 nm so that the critical volume v_c encompasses ~ 8 u.c. This estimate is of the same order as the radius circumscribed by the aforementioned assessment using the peak flexoelectric field isocontours from the FE simulations, thus reinforcing the assumption that the flexoelectric coefficients in the nanoscale are of the order of nC/m rather than of the order of μC/m. Flexoelectric coefficients of several orders of magnitude greater would have rendered markedly larger values for E_p and associated P in the FE simulations, sharply decreasing inferred r_c through Eq. (5). As a matter of fact, the calculated critical nucleus size would be an unrealistic and unphysical sub-atomic length.

Meanwhile, the simulations for sliding contact mode indicate that domain switching is simultaneously induced behind and underneath the AFM tip where the isocontour of maximum E_p is reached (Fig. 6). Regions of the film located in front and immediately underneath the sliding tip are however subjected to a strain gradient opposing domain expansion. As the material is placed behind the tip during sliding, the aforementioned strain gradients opposing domain switching are removed and hence a critical nucleated domain is allowed to expand. This produces overall switching across the film thickness. The role of the Coulombian friction coefficient μ is crucial in the proposed mechanism: a

decrease in μ gradually reduces the strain gradients that build in front and behind the tip, where the isocontours of flexoelectric field for normal and sliding modes converge at $\mu = 0$.

B. Tip-induced transition through the paraelectric phase

Under sufficient uniaxial compression, the tetragonality is so suppressed that a localized transition to the paraelectric phase is, in principle, possible. At the maximum applied load of 1000 nN, the top surface layer in contact with the AFM tip is subjected to an extreme triaxial stress field where the vertical compressive stress reaches $\sigma_{33} \sim$ -16 GPa and the transverse (radial) confining stress approximates to σ_{11} ($= \sigma_{22}$) ~ -11 GPa. The tetragonal structure is preserved in the top surface layer in contact with the AFM tip up to 900 nN because of the confinement provided by the aforementioned extreme radial compressive stresses. In contrast, in the central region of the film where the maximum value of E_{p} is located, we find $\sigma_{33} \sim$ -16 GPa and $\sigma_{11} \sim$ -2 GPa for the maximum applied load of 1000 nN. Superposition of the substrate-induced elastic misfit strain of -2.5×10^{-2} to such mechanical solicitations[16,29] results in vanishing tetragonality and transition towards the paraelectric phase in the central region of the film for applied loads in excess of ~ 400 nN. The results suggest that the inversion of polarization at the highest loads may be indirect and mediated through a biased paraelectric phase.

C. Influence of flexoelectric anisotropy and scaling issues

Another question concerns the relative weight of μ_{1111}, μ_{1122} and μ_{1212} when coupled to the specific strain gradients. We can rewrite Eq. (3) with the components of the polarization vector in Eq. (2), where

$$q = \mu_{1111} M_I + \mu_{1122} M_{II} + \mu_{1212} M_{III} \qquad \text{Eq. (6)}$$

and

$$M_I = e_{11,11} + e_{22,22} + e_{33,33} \quad , \qquad \text{Eq. (7a)}$$

$$M_{II} = e_{11,22} + e_{11,33} + e_{22,11} + e_{22,33} + e_{33,11} + e_{33,22} \, , \qquad \text{Eq. (7b)}$$

$$M_{III} = 4(e_{12,12} + e_{13,13} + e_{23,23}) \, . \qquad \text{Eq. (7c)}$$

Therefore, the coefficient μ_{1111} weights the derivative of normal strain gradients along the normal directions ($e_{ii,ii}$); μ_{1122} weights the derivative of normal strain gradients along transverse directions (the

specific above values of $e_{ii,jj}$); and μ_{1212} weights the derivative of the shearing strain gradients (the specific above values $e_{ij,ij}$). The results in Fig. 7 show that flexoelectric switching is fundamentally driven by the latter derivative of shear strain gradients (coupled to μ_{1212} through M_{III}). Only if coefficients μ_{1122} and μ_{1111} are about an order of magnitude greater than μ_{1212} will their influence in domain switching be comparable.

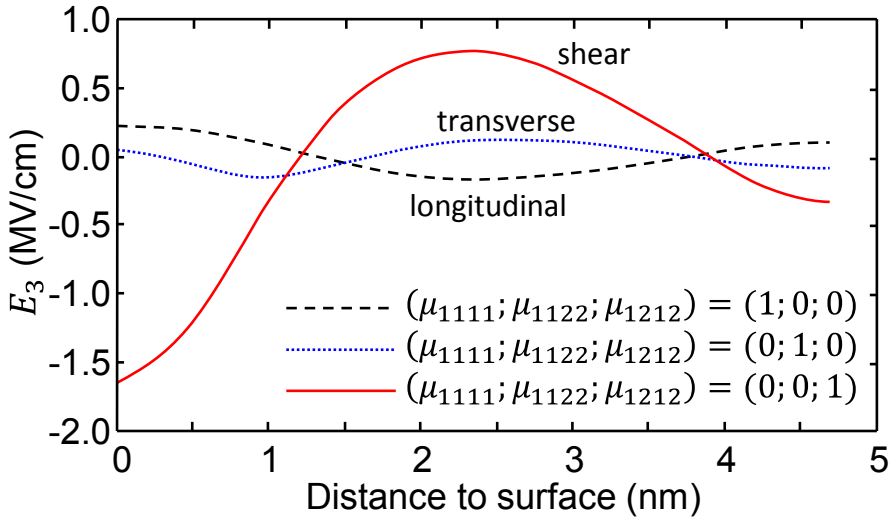

FIG. 7. (a) Distributions of the total electric field E3 along the vertical path underneath the contact center described in Fig. 5. The results are for 500 nN while the flexoelectric coefficients are systematically varied as shown in the legend. The results illustrate that flexoelectric nanocontacts are only sensitive to μ_{1212}.

An uncertainty in our modelling scheme concerns the role of surface piezoelectricity, which has been shown to be functionally equivalent to flexoelectricity.[10] This means that the employed flexoelectric coefficients are, in practice, the effective values that include both bulk flexoelectricity and surface piezoelectricity. From a quantitative point of view, of greater consequence is the fact that the model used here is not self-consistent: the strain gradient is calculated as a purely elastic problem without accounting for the fact that the elastic results would themselves be affected by the electric field. Strictly speaking, these values are mutually inter-dependent and should be calculated simultaneously as a coupled problem. The present model, however, still manages to transparently capture all the important

features of the problem, and good quantitative agreement with the experiment is obtained using realistic parameters.

The agreement between experiments and simulations is achieved for the flexoelectric coefficients in the order of 1–10 nC/m. Yet, in bulk $BaTiO_3$ ceramics, the reported experimental flexoelectric coefficients are of the order of 1–10 μC/m.[30] So, why is the flexoelectric coefficient of thin films so small? There is a concern that the flexoelectric coefficient of bulk ceramics is in fact anomalously large, and recent works suggest contribution of several extrinsic mechanisms to the total value.[11-13] Once these contributions are factored out, the intrinsic flexoelectric coefficient is a number of the order of 1-10 V multiplied by the permittivity of the material, i.e. $1–10 \times \varepsilon_r \varepsilon_0$.[10,30] For BTO ceramics, the relative permittivity is of the order of ε_r=1000–30000 depending on the proximity to the ferroelectric phase transition, and thus the flexoelectric coefficient that one should expect in bulk is of the order of ~0.1 μC/m, which is still about 100 times greater than we observe in our films.

These results, however, can be readily reconciled by observing that the relative permittivity along the c-axis for BTO thin films epitaxially clamped on STO substrates is much smaller than for bulk: according to Landau theory calculations it is of the order of 30-50.[16] Also, note that the value ε_r = 30 used in the present simulations yielded a good agreement with the experiment. Hence, the riddle is solved: while the flexoelectric coefficient of our films seems anomalously small in comparison with bulk, the *flexocoupling* coefficient (flexoelectric coefficient divided by permittivity, which is the property that fundamentally relates the strain gradients to the electric field) is still the same, namely, a number between 1–10 V. This means that since the permittivity of thin films is much smaller than that of the bulk materials,[32,33] the flexoelectric response is preserved in the nanoscale. Maximizing flexoelectricity at the nanoscale thus requires maximizing the dielectric susceptibility.

V. CONCLUSIONS

The present comprehensive study of the experimental and theoretical aspects of flexoelectric switching yields several non-trivial and important conclusions. Below we summarize them:

1) In perpendicular load experiments, a ferroelectric domain is nucleated when a critical strain gradient is achieved in a sufficiently large volume fraction of the material. However, the produced domain is unstable due to the existence of a surface layer where the strain gradient has the opposite sign of that at the region below.
2) In the sliding contact load regime, due to the presence of the tangential strain gradient, the region in the wake of the tip has a net downward flexoelectric field that is not cancelled by any inversion layer. Hence, the switching can be realized at lower applied mechanical loads in the sliding regime, where domain growth proceeds unimpeded and stable domains can be formed.
3) At sufficiently large loading forces (≥400 nN), the switching from the upward to the downward polarization may proceed through an intermediate transition to the paraelectric phase, caused by the large vertical compression exerted by the tip.
4) The obtained results are consistent with flexoelectric coefficients being of the order of a few nC/m, in contrast to the μC/m in bulk BTO ceramics. Yet, when dividing these coefficients by the permittivity, the *flexocoupling* coefficients of the films are of the order of 1–10 V, which is the same as in bulk.

Though strain gradients can effectively replace voltage in order to switch ferroelectric polarization, the mechanically-induced field distribution is very different from that, which would arise from just electrostatic voltage, and has to be exploited differently. In particular, while electrostatic domain switching with a static contact is possible, mechanical switching requires the larger shear stresses associated with sliding contacts – in other words, mechanical writing of lines or dashes is easier than writing of dots. Similarly, the scaling of flexoelectricity and permittivity means that one cannot automatically assume bulk values. Making efficient nanoscale flexoelectric devices requires not just careful strain gradient engineering, but also careful materials science in order to ensure the material properties are optimally translated to the nanoscale.

ACKNOWLEDGEMENTS

We thank Prof. Massimiliano Stengel for insightful discussions. The work at the UNL was supported by the National Science Foundation (NSF) through the Nebraska Materials Research Science

and Engineering Center (MRSEC) under Grant No DMR-1420645 (PFM experiments) and by the US Department of Energy, Office of Science, Basic Energy Sciences, Division of Materials Sciences and Engineering, under Award DE-SC0004876 (fabrication of thin films). The work of G.C. is financially supported by an ERC grant (project number 308023), by a National Plan grant (FIS2013-48668-C2-1-P) and by the Severo Ochoa Excellence programme. Further financial support was provided by Ministerio de Economía y Competitividad Grant MAT2011-23375 (Spain) to J.A. and by CENTEM projects CZ.1.05/2.1.00/03.0088 and PLUS LO1402 (Czech Republic) to J.O.

APPENDIX

Using the symmetry considerations by Shu[34] for cubic crystals, Eq. (1) can be strictly simplified as

$$P_i = \mu_{in} e_n \,,$$

where

$$\mu_{in}^{(3\times18)} = \begin{pmatrix} \mu_{1111} & 0 & 0 & \mu_{1122} & 0 & 0 & \mu_{1122} & 0 & 0 & 0 & 2\mu_{1212} & 0 & 0 & 0 & 2\mu_{1212} & 0 & 0 & 0 \\ 0 & \mu_{1122} & 0 & 0 & \mu_{1111} & 0 & 0 & \mu_{1122} & 0 & 2\mu_{1212} & 0 & 0 & 0 & 0 & 0 & 0 & 0 & 2\mu_{1212} \\ 0 & 0 & \mu_{1122} & 0 & 0 & \mu_{1122} & 0 & 0 & \mu_{1111} & 0 & 0 & 0 & 2\mu_{1212} & 0 & 0 & 0 & 2\mu_{1212} & 0 \end{pmatrix}$$

and

$$e_n^{(18\times1)} = \left(e_{11,1}\ e_{11,2}\ e_{11,3}\ e_{22,1}\ e_{22,2}\ e_{22,3}\ e_{33,1}\ e_{33,2}\ e_{33,3}\ e_{12,1}\ e_{12,2}\ e_{12,3}\ e_{13,1}\ e_{13,2}\ e_{13,3}\ e_{23,1}\ e_{23,2}\ e_{23,3}\right).$$

This directly yields Eqs. 2a, 2b and 2c from the main text.

REFERENCES

[1] H. Lu, C.-W. Bark, D. Esque De Los Ojos, J. Alcala, C. Eom, G. Catalan and A. Gruverman, "Mechanical writing of ferroelectric polarization," *Science,* vol. 335, no. 6077, pp. 59-61, 2012.

[2] S. Kogan, "Piezoelectric effect during inhomogeneous deformation and acoustic scattering of carriers in crystals," *Sov. Phys. Solid State,* vol. 5, pp. 2069-2070, 1964.

[3] G. Catalan, L. Sinnamon and J. Gregg, "The effect of flexoelectricity on the dielectric properties of inhomogeneously strained ferroelectric thin films," *Journal of Physics Condensed Matter,* vol. 16, no. 13, pp. 2253-2264, 2004.

[4] G. Catalan, A. Lubk, A. Vlooswijk, E. Snoeck, C. Magen, A. Janssens, G. Rispens, G. Rijnders, D. Blank and B. Noheda, "Flexoelectric rotation of polarization in ferroelectric thin films," *Nature Materials,* vol. 10, no. 12, pp. 963-967, 2011.

[5] D. Lee, A. Yoon, S. Jang, J.-G. Yoon, J.-S. Chung, M. Kim, J. Scott and T. Noh, "Giant flexoelectric effect in ferroelectric epitaxial thin films," *Physical Review Letters,* vol. 107, no. 5, 2011.

[6] E. V. Bursian and O. I. Zaikovskii, "Changes in the curvature of a ferroelectric film due to polarization," *Sov. Phys. Solid State,* vol. 10, pp. 1121-1124, 1968.

[7] L. Cross, "Flexoelectric effects: Charge separation in insulating solids subjected to elastic strain gradients," *Journal of Materials Science,* vol. 41, no. 1, pp. 53-63, 2006.

[8] A. Tagantsev, V. Meunier and P. Sharma, "Novel Electromechanical Phenomena at the Nanoscale: Phenomenological Theory and Atomistic Modeling," *MRS Bulletin,* vol. 34, no. 9, pp. 643-647, 2009.

[9] W. Ma, "A study of flexoelectric coupling associated internal electric field and stress in thin film ferroelectrics," *Physica Status Solidi (B) Basic Research,* vol. 245, no. 4, pp. 761-768, 2008.

[10] P. Zubko, G. Catalan and A. Tagantsev, "Flexoelectric effect in solids," *Annual Review of Materials Research,* vol. 43, pp. 387-421, 2013.

[11] J. Narvaez and G. Catalan, "Origin of the enhanced flexoelectricity of relaxor ferroelectrics," *Applied Physics Letters,* vol. 104, no. 16, p. 162903, 2014.

[12] A. Biancoli, C. M. Fancher, J. L. Jones and D. Damjanovic, "Breaking of macroscopic centric symmetry in paraelectric phases of ferroelectric materials and implications for flexoelectricity," *Nat Mater,* vol. 14, no. 2, pp. 224-229, 2015.

[13] I. Bersuker, "Pseudo Jahn-Teller effect in the origin of enhanced flexoelectricity," *Applied Physics Letters,* vol. 106, no. 2, p. 022903, 2015.

[14] L. Garten and S. Trolier-Mckinstry, "Enhanced flexoelectricity through residual ferroelectricity in barium strontium titanate," *Journal of Applied Physics,* vol. 117, no. 9, p. 094102, 2015.

[15] K. Choi, M. Biegalski, Y. Li, A. Sharan, J. Schubert, R. Uecker, P. Reiche, Y. Chen, X. Pan, V. Gopalan, L.-Q. Che, D. Schlom and C. Eom, "Enhancement of ferroelectricity in strained BaTiO3 thin films," *Science,* vol. 306, no. 5698, pp. 1005-1009, 2004.

[16] A. Emelyanov, N. Pertsev and A. Kholkin, "Effect of external stress on ferroelectricity in epitaxial thin films," *Physical Review B,* vol. 66, no. 21, pp. 2141081-2141088, 2002.

[17] A. Dent, C. Bowen, R. Stevens, M. Cain and M. Stewart, "Effective elastic properties for unpoled barium titanate," *Journal of the European Ceramic Society,* vol. 27, no. 13-15, pp. 3739-3743, 2007.

[18] T. Darling, A. Migliori, E. Moshopoulou, S. Trugman, J. Neumeier, J. Sarrao, A. Bishop and J. Thompson, "Measurement of the elastic tensor of a single crystal of La0.83Sr0.17MnO3 and its response to magnetic fields," *Physical Review B - Condensed Matter and Materials Physics,* vol. 57, no. 9, pp. 5093-5097, 1998.

[19] M. Mata and J. Alcala, "The role of friction on sharp indentation," *Journal of the Mechanics and Physics of Solids,* vol. 52, no. 1, pp. 145-165, 2004.

[20] O. Braun and A. Naumovets, "Nanotribology: Microscopic mechanisms of friction," *Surface Science Reports,* vol. 60, no. 6-7, pp. 79-158, 2006.

[21] Y. Mo, K. Turner and I. Szlufarska, "Friction laws at the nanoscale," *Nature,* vol. 457, no. 7233, pp. 1116-1119, 2009.

[22] J. Hong, G. Catalan, J. Scott and E. Artacho, "The flexoelectricity of barium and strontium titanates from first principles," *Journal of Physics Condensed Matter,* vol. 22, no. 11, p. 112201, 2010.

[23] R. Maranganti and P. Sharma, "Atomistic determination of flexoelectric properties of crystalline dielectrics," *Physical Review B - Condensed Matter and Materials Physics,* vol. 80, no. 5, p. 054109, 2009.

[24] A. Gruverman, D. Wu, and J. F. Scott, “Piezoresponse Force Microscopy Studies of Switching Behavior of Ferroelectric Capacitors on a 100-ns Timescale”, *Phys. Rev. Lett*. **100**, p. 097601, 2008.

[25] J. Jo, D. Kim, Y. Kim, S.-B. Choe, T. Song, J.-G. Yoon and T. Noh, "Polarization switching dynamics governed by the thermodynamic nucleation process in ultrathin ferroelectric films," *Physical Review Letters,* vol. 97, no. 24, p. 247602, 2006.

[26] J. Jo, Y. Kim, T. Noh, J.-G. Yoon and T. Song, "Coercive fields in ultrathin BaTiO3 capacitors," *Applied Physics Letters,* vol. 89, no. 23, p. 232909, 2006.

[27] J. F. Scott, Ferroelectric Memories, Sprnger-Verlag Berlin Heidelberg, 2000.

[28] J. Padilla, W. Zhong and V. D., "First-principles investigation of 180° domain walls in BaTiO3," *Physical Review*

B, vol. 53, no. 10, pp. 5969-5973, 1996.

[29] O. Diéguez, K. Rabe and D. Vanderbilt, "First-principles study of epitaxial strain in perovskites," *Physical Review B - Condensed Matter and Materials Physics,* vol. 72, no. 14, p. 144101, 2005.

[30] W. Ma and L. Cross, "Flexoelectricity of barium titanate," *Applied Physics Letters,* vol. 88, no. 23, p. 232902, 2006.

[31] I. Ponomareva, A. Tagantsev and L. Bellaiche, "Finite-temperature flexoelectricity in ferroelectric thin films from first principles," *Physical Review B - Condensed Matter and Materials Physics,* vol. 85, no. 10, p. 104101, 2012.

[32] M. Saad, P. Baxter, R. Bowman, J. Gregg, F. Morrison and J. Scott, "Intrinsic dielectric response in ferroelectric nano-capacitors," *Journal of Physics Condensed Matter,* vol. 16, no. 41, pp. L451-L456, 2004.

[33] M. Stengel and N. Spaldin, "Origin of the dielectric dead layer in nanoscale capacitors," *Nature,* vol. 443, no. 7112, pp. 679-682, 2006.

[34] L. Shu, X. Wei, T. Pang, X. Yao, and C. Wang, “Symmetry of flexoelectric coefficients in crystalline medium,” J. Appl. Phys. 110, 104106, 2011.